Regional Shear Wave Speeds Track Regional Axial Stress in Nonuniformly Loaded Fibrous Soft Tissues

Jonathon L. Blank
Department of Mechanical Engineering, University of Wisconsin-Madison, Madison, WI
1513 University Avenue Room 3046, Madison, WI 53726
jlblank@wisc.edu

Darryl G. Thelen
Department of Mechanical Engineering, University of Wisconsin-Madison, Madison, WI
Department of Biomedical Engineering, University of Wisconsin-Madison, Madison, WI
1513 University Avenue Room 2107, Madison, WI 53726
dgthelen@wisc.edu

Joshua D. Roth
Department of Mechanical Engineering, University of Wisconsin-Madison, Madison, WI
Department of Orthopedics and Rehabilitation, University of Wisconsin-Madison, Madison, WI
1111 Highland Avenue Room 5009, Madison, WI 53706
roth@ortho.wisc.edu

Keywords: Tendon; ligament; shear wave tensiometry; nonuniform loading; regional axial stress; regional tissue mechanics; finite element model

ABSTRACT

Ligaments and tendons undergo nonuniform deformation during movement. While deformations can be imaged, it remains challenging to use such information to infer regional tissue loading. Shear wave tensiometry is a promising noninvasive technique to gauge axial stress and is premised on a tensioned beam model. However, it is unknown whether tensiometry can predict regional stress in a nonuniformly loaded structure. The objectives of this study were to (1) determine the relationship between regional shear wave speed and regional axial stress, and (2) determine the sensitivity of regional axial stress and regional shear wave speed measurements to nonuniform load distribution and fiber alignment in the presence of variable tissue geometry and constitutive properties. We created a representative set of 12,000 dynamic finite element models of a fibrous soft tissue with probabilistic variations in fiber alignment, stiffness, and aspect ratio. In each model, we applied a randomly selected, nonuniform load distribution, and then excited a shear wave and tracked its *regional propagation. We found that regional shear wave speed was an excellent predictor of the regional axial stress (RMSE=0.55 MPa) and that the nature of the wave speed-stress relationship was consistent with a tensioned beam model (R^2 = 0.99). Variations in tissue geometry, nonuniform loading, fiber material properties, and fiber alignment did not substantially alter the wave speed-stress relationship, particularly at higher loads. Thus, these finding suggests that shear wave tensiometry could provide for a quantitative estimate of regional tissue stress in ligaments and tendons.*

1. INTRODUCTION

Ligaments and tendons undergo complex deformation during movement. For example, joint motion can induce nonuniform ligament stretch due to rotation of the ligament's attachments on adjacent bone segments (Robinson et al. 2004; Willinger et al. 2020). Nonuniform deformation is also observed in tendinous tissue which can undergo heterogenous muscle loading (Franz et al. 2015). The capacity of ligaments and tendons to change shape and effectively transmit loads is critical to normal biomechanical function. Interfibrillar sliding is a structural factor that may further facilitate nonuniform deformation (Szczesny and Elliott 2014), and the degree of fiber alignment can affect the relative amounts of sliding and shear load transmission that occurs. For example, ligament fibers are relatively less aligned than in tendon (Amis 1998; Wymenga et al. 2006), which is believed to provide for complex load transmission about a joint.

Assessing nonuniform loading remains a challenge in biomechanical assessments of soft tissue mechanics. Currently, digital image correlation is the gold standard technique for gauging strain distributions (Mallett and Arruda 2017). In combination with material-informed finite element models, one can predict stress distributions in tendon and ligament (Readioff et al. 2020). Such measurements clearly demonstrate the complex mechanics of the tissue in response to an anatomical load (J C Gardiner and Weiss 2003). However, it remains challenging to verify these model-based stress estimates due to the paucity of techniques for measuring regional stress.

Shear wave speeds are widely used to study musculoskeletal tissue mechanics (J. Blank et al. 2022) . A tensioned beam models suggests that the speed of the propagating shear wave is proportional to the square root of axial tissue stress (Martin et al. 2018). This general relationship is shown to hold for ligament (J. L. Blank, Thelen, and Roth 2020a) and tendon (Martin et al. 2019) under pure axial loading. However, it is uncertain whether the wave speed-stress relationship holds in a tissue undergoing nonuniform loading. We previously used a probabilistic, dynamic finite element model to investigate the effects of fiber alignment and material properties on shear wave speeds in ligaments and tendons (J. L. Blank et al. 2021). This study extends that work by considering nonuniform deformations that can arise in a ligament due to joint rotation. Accordingly, the objectives of this study were to, (1) determine the relationship between regional shear wave speed and regional axial stress, and (2) determine the sensitivity of regional axial stress and regional shear wave speed measurements to nonuniform load distribution and fiber alignment in the presence of variable tissue geometry and constitutive properties.

2. METHODS

2.1. Finite Element Model Overview

We implemented a previously validated finite element model capable of simulating dynamic shear wave propagation in a fibrous soft tissue during nonuniform loading (J. L. Blank et al. 2021) (Fig. 1). The tissue was modeled as a 60 mm-long ellipse with a predefined width and thickness. The tissue was composed of a mesh with 3,600 hexahedral elements, which was prescribed under guidance of a prior mesh convergence study (J. L. Blank et al. 2021). The proximal end of the tissue was attached to a rigid body capable of being loaded with unequal tensions on each side to create a nonuniform load distribution (Fig. 1a).

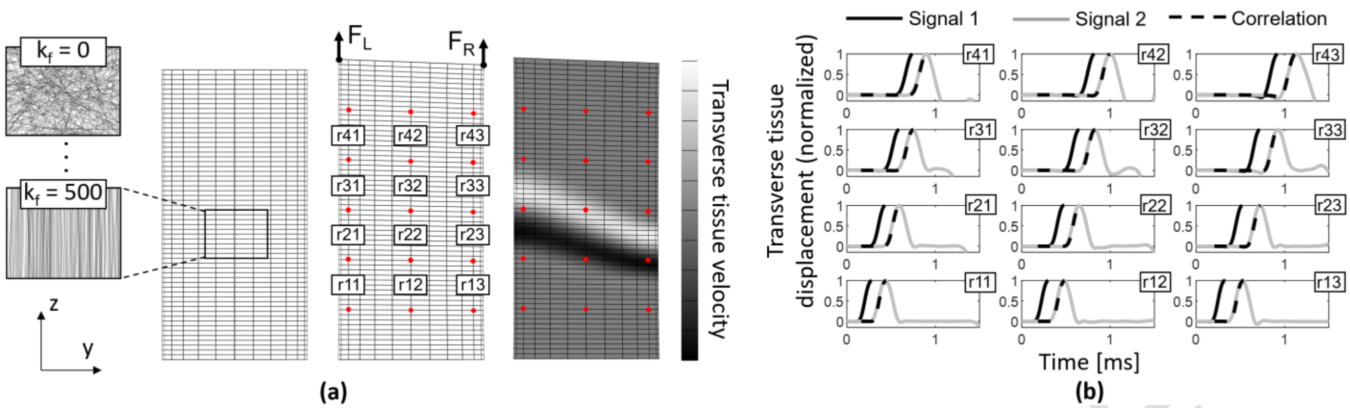

Figure 1: (a) We modeled the tissue as transversely isotropic with distributed fibers in the YZ plane. We first nonuniformly loaded the tissue in the static simulation using two point loads on either side of the proximal rigid body. We then excited a shear wave at the bottom of the tissue and let it propagate in a dynamic simulation. **(b)** We monitored the transverse tissue motion at each point across the tissue width and length and measured a shear wave speed in each region (12 shear wave speeds total per simulation).

2.2. Constitutive Model

We modeled the tissue as an incompressible, transversely isotropic hyperelastic material with distributed fibers that represents a material with longitudinal fibers embedded in a matrix using the following combination of strain energy density functions (Eq. 1):

$$\Psi = \Psi_{matrix} + \Psi_{fibers} \tag{1}$$

Here, Ψ_{matrix} represents the contribution of the ground matrix, which governs the transverse shear modulus, and Ψ_{fibers} represents the contribution of embedded fibers. The ground matrix was isotropic according to a Mooney-Rivlin constitutive model ($C_1 = C_2 = 0.205$ MPa). The ground matrix, embedded fibers, and tissue's volumetric response to loading were characterized using the following uncoupled strain energy density function, Ψ (Eq. 2):

$$\Psi = F_1(\tilde{I}_1, \tilde{I}_2) + \int_{\theta_p - \frac{\pi}{2}}^{\theta_p + \frac{\pi}{2}} P(\theta)\, F_2\big(\tilde{\lambda}[\theta]\big)\, d\theta + \frac{K}{2}(ln J)^2 \qquad (2)$$

$\tilde{I}_1$ and $\tilde{I}_2$ represent the first and second invariants of the right Cauchy-Green deformation tensor, $\tilde{\lambda}$ indicates the deviatoric part of the stretch ratio along the fiber direction, K represents the bulk modulus, and finally J represents the volume change of the deformation. The parameter θ is indicative of changes in fiber alignment according to the 2D unimodal distribution function, P(θ) (Eq. 3):

$$P(\theta) = \frac{1}{\pi I_0 k_f} e^{k_f \cos\left(2(\theta - \theta_p)\right)} \qquad (3)$$

The principal fiber orientation, θ_p, represents the nominal fiber angle and was chosen to align with the longitudinal axis of the tissue (defined from positive z-axis in YZ-plane, Figure 1). I_0 represents the modified Bessel function of the first kind, and the fiber concentration factor, k_f, determines the degree of fiber alignment within the tissue. Fiber concentration values from 0 to 100 were chosen to represent highly unaligned (i.e., isotropic) and highly aligned (i.e., transversely isotropic) fibers, respectively (Stender et al. 2018). $F_2(\tilde{\lambda})$ represents the contribution of the collagen fibers to the strain energy density function (Eq. 4):

$$\begin{aligned} \tilde{\lambda}\frac{\partial F_2}{\partial \tilde{\lambda}} &= 0 && \tilde{\lambda} \leq 1 \\ \tilde{\lambda}\frac{\partial F_2}{\partial \tilde{\lambda}} &= C_3 e^{C_4(\tilde{\lambda}-1)} - 1 && 1 < \tilde{\lambda} \leq \lambda^* \\ \tilde{\lambda}\frac{\partial F_2}{\partial \tilde{\lambda}} &= C_5\tilde{\lambda} + C_6 && \tilde{\lambda} > \lambda^* \end{aligned} \qquad (4)$$

Here, $\tilde{\lambda}$ represents the tissue stretch during loading, and λ^* is the stretch at which the fibers engage. Prior to this stretch level, the fibers are either slack or uncrimping, where the term C_3 scales the exponential stress and the term C_4 controls the strain-dependent rate at which the fibers uncrimp. The term C_5 corresponds to the elastic modulus of straightened fibers and C_6 is determined using the requirement that the stress-strain curve be continuous at λ^*. For a transversely isotropic material, the stretch of the collagen fibers is the same as $\tilde{\lambda}$, which is a function of deformation in the z-direction. For tissues with unaligned fibers, this response is scaled using the 2D unimodal distribution function.

2.3. Probabilistic Model Parameters

We generated 12,000 models with variable tissue geometry (§2.3.1.), nonuniform loading (§2.3.2.), and fiber stiffness and alignment (§2.3.3.) as a representative cohort for variations in musculoskeletal soft tissues in human patients (Table 1).

Table 1: Ranges of parameters varied in our cohort of models with probabilistic variations in geometry, boundary conditions, hyperelastic material properties, and microstructure.

Probabilistic Model Category	Parameter description	Parameter	Value
Tissue geometry	Tissue thickness	w [mm]	3-6
	Tissue width	t [mm]	6-30
Nonuniform load	Nonuniform load distribution	ΔF [N]	0-100
	Axial load	F [N]	0-600
Fiber stiffness	Toe region stress term	C_3 [MPa]	0.1 – 1.5
	Toe region uncrimping term	C_4	30 – 70
	Linear region modulus	C_5 [MPa]	300 - 900
Fiber alignment	Fiber alignment factor	k_f	0-100

2.3.1. Tissue Geometry Parameters

We evaluated the sensitivity of load distribution and regional shear wave speeds to tissue geometry by varying the tissue's thickness from 3 to 6 mm and the width from 6 to 30 mm according to a random uniform distribution. The tissue was held to a constant width and thickness along the entire length.

2.3.2. Nonuniform Load Distribution

We generated nonuniform loads to evaluate the capability of regional shear wave speed to track regional axial stress during different loading conditions. We varied the axial load on the either side of the model from 0 to 300 N according to a random uniform distribution. We ensured that the difference in load between the two sides of the tissue did not exceed 100 N.

2.3.3. Fiber Alignment and Fiber Stiffness

We systematically varied fiber alignment and stiffness to assess their effects on regional loading and the resultant regional shear wave propagation. We varied fiber alignment by varying the value of k_f from 0 to 100 according to a positive, one-sided normal distribution (mean = 0, standard deviation = 25). Our one-sided normal distribution was selected to reflect the non-linear decreasing effect of fiber alignment on mechanics as k_f is increased (J. L. Blank et al. 2021). We also varied fiber stiffness using the constitutive model constants C_3 (toe-region exponential stress coefficient), C_4 (rate of fiber uncrimping), and C_5 (linear region modulus). Fiber material properties were varied according to a random uniform distribution (Table 1).

2.4. Simulation of Shear Wave Propagation under Nonuniform Loading

We simulated shear wave speeds using a previously validated finite element (FE) modeling framework (J. L. Blank, Thelen, and Roth 2020b; J. L. Blank et al. 2021). All finite element simulations were performed in FEBio version 3.0 (Maas et al. 2012). The bottom surface of the structure was held fixed. In the initial, static portion of the simulation, we loaded the rigid grip with unequal tensions on both sides by applying a predefined force to one node on each end of the grip (Fig. 1). During the dynamic portion of the simulation, we excited a shear wave in the model by applying a transverse displacement ramp of 10 microns at 2 kHz to nodes through the model's cross-section (Fig. 1). The excitation displacement and timing were chosen to match the excitation signal of current voice coilactuated tensiometer designs. Following the excitation, the shear wave was allowed to propagate along the structure for 2.5 ms. We executed all our simulations on a high-throughput computing grid.

We measured regional shear wave speeds according to prior finite element modeling studies (J. L. Blank et al. 2021). Briefly, we monitored transverse tissue motion at locations both along the length and width of the tissue (Fig. 1). The shear wave travel time was determined using a normalized cross-correlation of the transverse displacement profiles two consecutive measurement points (1 cm distance) along the structure's long-axis. Cosine interpolation was used to assess sub-sample alignment of the displacement profiles (Cespedes et al. 1995). Transverse wave profiles having a correlation strength of less than 0.75 were excluded due to signal decorrelation. Shear wave speed was then computed as the distance between measurement nodes divided by the wave travel time. We measured the corresponding regional axial stress as the average axial Cauchy stress at elements between the two measurement points. Shear wave speeds less than 15 m/s or greater than 160 m/s were considered out of range of our tensioned beam model and were excluded. We retained over 96.5% of the 12,000 simulations for our analyses.

2.5. Statistical Analysis

For our first objective, we assessed the relationship between the regional shear wave speed and regional axial stress using a linear regression according to the following analytical relationship (Martin et al. 2018) (Eq. 5):

$$\sigma = \rho_{eff} c^2 - k'\mu \tag{5}$$

Here, σ represents the axial tendon stress (in Pa), ρ_{eff} the effective density of the propagation medium (in kg/m^3), c the shear wave speed (in m/s), k' a shear correction factor (unitless), and μ the tangential shear modulus of the tissue (in Pa). We compared shear wave speeds to the tensioned beam model evaluated using the material properties set for the FE model (ρ_{eff} = 1500 , μ = 0.82 MPa, k'= 0.89), and also used the linear relationship of the tensioned beam model to determine the axial stress given shear wave speed and linear regression coefficients. For all linear regressions, the dependent variable was the regional axial stress, σ, and the independent variable was the squared regional shear wave speed, c^2. Errors between the predicted and actual regional stresses are denoted as ε (in MPa).

To perform our sensitivity analyses stated in our second objective, we first performed a multiple linear regression with one-way interactions between the one of the response variables (i.e., regional stress distribution or stress prediction error) and two of the independent variables (i.e., *w*, *t*, ΔF, *F*, C_3, C_4, C_5, or k_f from Table 1) (Eq. 6):

$$y = \alpha + \beta_1 x_1 + \beta_2 x_2 + \beta_3 x_1 x_2 + \varepsilon \tag{6}$$

Here, y represents the one of the response variables (i.e., either regional stress distribution or stress prediction error), x_1 and x_1 represent the two of the independent variables (i.e., *w*, *t*, ΔF, *F*, C_3, C_4, C_5, or k_f), and β_{1-3} represent the regression coefficients that we used to define sensitivity for each parameter. We also performed a linear regression between each independent variable (i.e., *w*, *t*, ΔF, *F*, C_3, C_4, C_5, or k_f) and response variable (i.e., regional stress distribution or stress prediction error). Interactions that accounted for more variance in the response variable (i.e., had higher R^2) were considered important.

3. RESULTS

3.1. Regional Shear Wave Speeds Predict Regional Axial Stress

We observed regional stress distributions that were dependent on the tissue's fiber alignment. More specifically, less well-aligned fibers corresponded to a more evenly distributed regional stress distribution, and tissues with highly aligned fibers had increased differences in axial stress magnitudes across the tissue width (Fig. 2a-b). Regional shear wave propagation speed scaled with increases in regional axial stress (Fig. 2c).

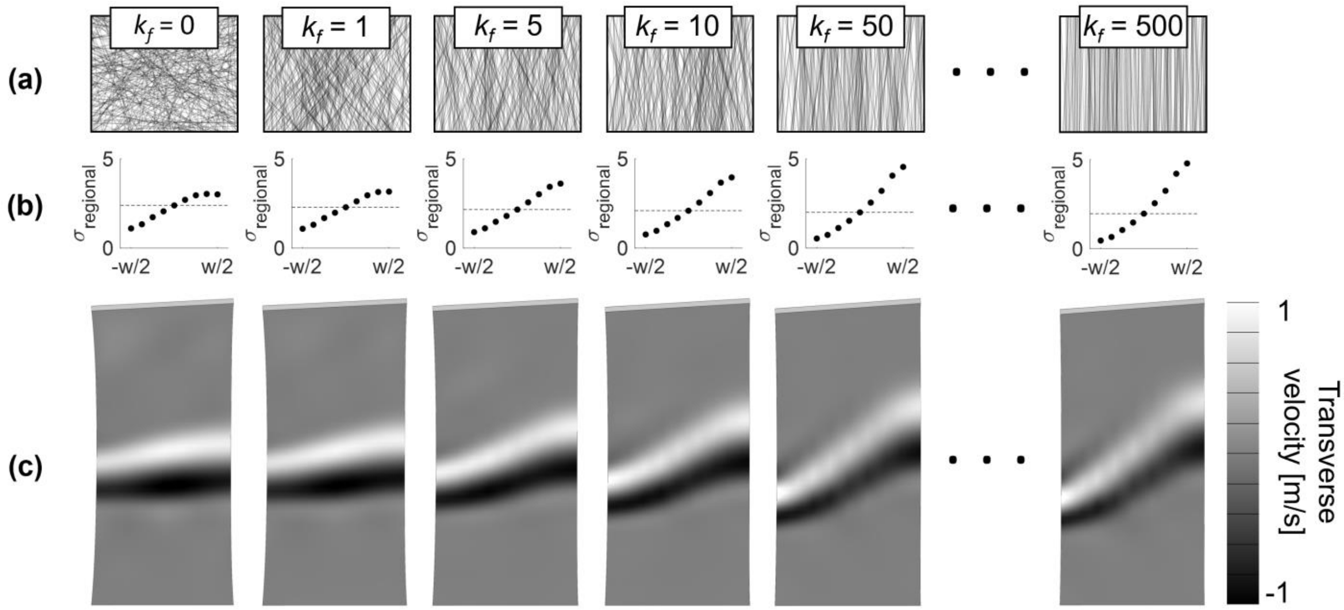

Figure 2: (a) Images representing fiber alignment factors (k_f) ranging from 0 (random alignment) to 500 (highly aligned). **(b)** Axial stress distributions over the width of the structure when subject a 100-N load differential from left to right and a total axial load of 300 N. **(c)** Shear wave propagation in response to a transverse excitation of the bottom of the nonuniformly loaded structure. Wave speed across the width varied substantially as fibers became more aligned.

Regional shear wave speed scaled with regional stress. We found that regional shear wave speed squared was an excellent predictor of the regional axial stress (RMSE = 0.55 MPa, R^2 = 0.99), and that regional shear wave speeds measured in the model agreed well with those predicted using the tensioned beam model with applied model parameters (p_{eff} = 1500 kg/m^3, μ = 0.82 MPa) (Fig. 3). Correspondingly, regional wave speed was not nearly as good at predicting average tendon stress ($\sigma_{average} = F/A$), with prediction errors that doubled when using regional shear wave speeds (RMSE = 1.11 MPa, R^2 = 0.93) (Fig. 4b). Generally higher errors in regional stress predictions were observed for high nonuniform load distributions in low stress regions. High nonuniform load distributions resulted in higher average stress prediction errors independent of load level.

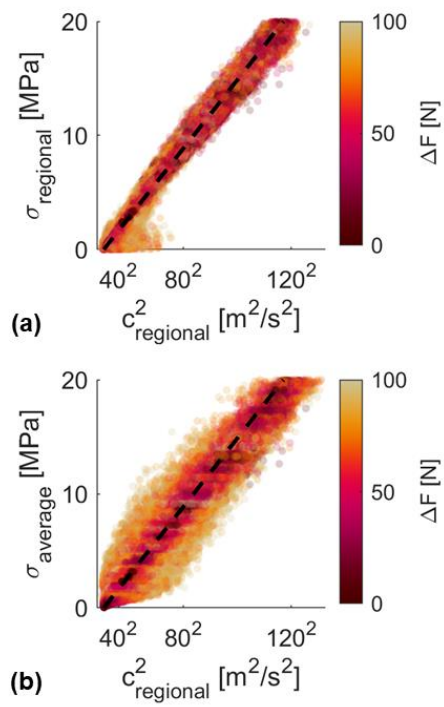

Figure 3: Regional shear wave speed was a better predictor of the regional axial stress **(a)** (RMSE = 0.55 MPa, R^2 = 0.99) than the average axial stress **(b)** (RMSE = 1.11 MPa, R^2 = 0.93) in tissues undergoing increasing nonuniform load (as indicated by the colormap).

3.2. Fiber Alignment Facilitates Axial Stress Transmission Across the Tissue

Our simulations revealed that nonuniform load distribution (ΔF) was an important factor for determining the regional stress distribution (R^2 = 0.74) (Fig. 4). Among these factors, we determined that the interaction between nonuniform load distribution and fiber alignment accounted for 85% of the variability in regional stress under nonuniform loading (Fig. 5). We also determined that interactions between thickness and nonuniform load distribution accounted for 82% of the variability in regional stress (Fig. 3S). We did not find that other parameters (i.e., w, F, C_3, and C_4) influenced regional stress distributions by themselves, and that no other interactions increased the sensitivity of regional stress distribution. All sensitivities and interactions are included in the Electronic Supplementary Materials (Fig. 3S).

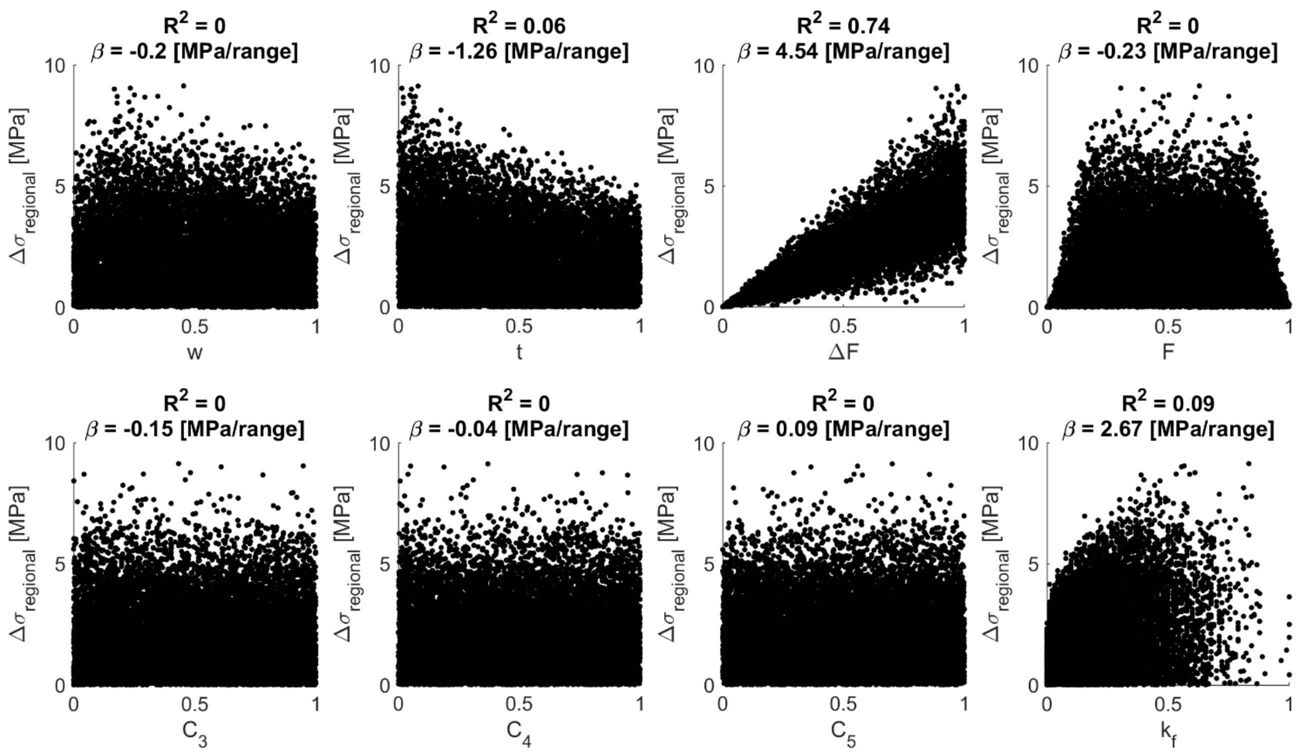

Figure 4: Sensitivity of regional stress distribution, $\Delta\sigma_{regional}$ to normalized parameter ranges. Shown are the percentage of variability of $\Delta\sigma_{regional}$ accounted for by a single parameter (R^2), and the slope of a linear regression fit (in MPa/parameter range). Parameter ranges are given in Table 1.

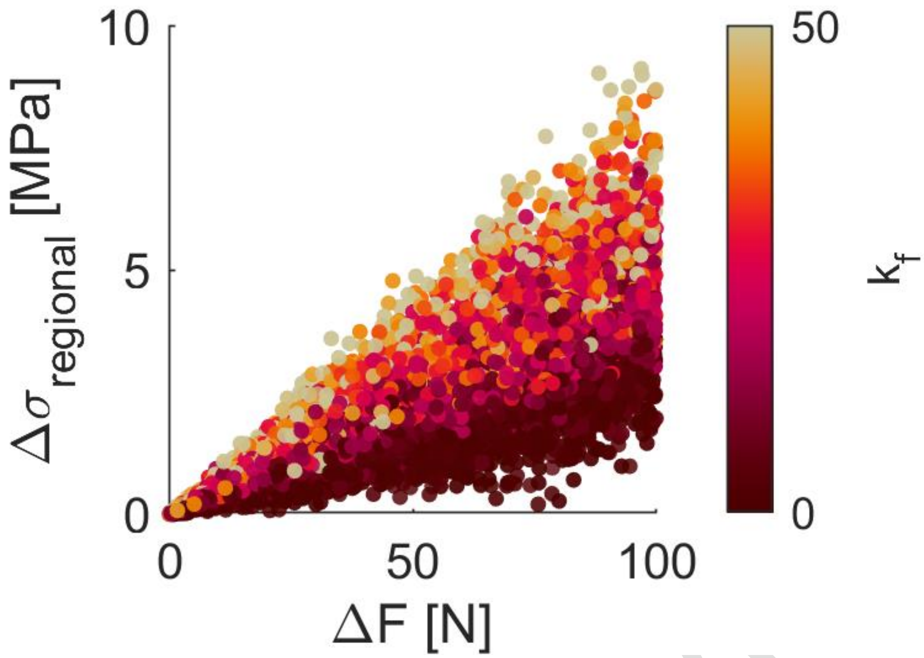

Figure 5: Interaction between the nonuniform load distribution, *ΔF*, and the fiber alignment factor, k_f, resulted in predictable variations in the regional stress distribution across the tissue width.

3.3. Regional Axial Stress Predictions are Insensitive to Probabilistic Tissue Factors

When predicting the regional axial stress using the regional shear wave speed, we found that no individual parameter accounted for more than 4% of the variability in regional stress prediction errors. We found that interactions between geometric terms (*t, w*), load terms (*ΔF*, *F*), and fiber alignment (k_f) accounted for more variability in regional stress prediction errors, but no grouping of variables accounted for more than 8% of the variability observed. By themselves, fiber alignment and stiffness terms had no effect on regional stress prediction errors ($R^2 = 0$). All sensitivities and interactions are included in the Electronic Supplementary Materials (Fig. 4-5S, Table 1S).

4. DISCUSSION

The objectives of this study were to (1) determine the relationship between regional shear wave speed and regional axial stress, and (2) determine the sensitivity of regional axial stress and regional shear wave speed measurements to nonuniform load distribution and fiber alignment in the presence of variable tissue geometry and constitutive properties. Our first key finding was that regional shear wave speed tracks regional axial stress in a manner that is well described by a tensioned beam model(Martin et al. 2018). Our second key finding was that nonuniform fiber alignment acted to distribute axial stress across the tissue leading to more uniform regional stresses during nonuniform loading. Our last key finding was that the accuracy of axial stress predictions made using shear wave speed were generally independent of tissue geometry, nonuniform load, fiber material properties, and fiber alignment.

Concerning our first objective, we found that regional shear wave speeds are an excellent predictor of the regional axial stress (Fig. 3). Based on a tensioned beam model, shear wave speed was previously shown to be a good predictor of axial stress in an axially loaded fibrous tissues (Martin et al. 2018). We were motivated to consider nonuniform loading scenarios given that ligaments routinely undergo nonuniform deformations due to joint motion. Our model results suggest that shear wave speed may be a good predictor of regional tissue stress under such conditions. The regional wave speed-stress relationships were relatively independent of fiber alignment and fiber linear region stiffness (§3.3.), particularly at higher loads (J. L. Blank et al. 2021). We found that regional wave speed-stress relationships were instead dependent on the extent of nonuniform loading in the tissue. More specifically, we observed diminished capacity of regional shear wave speeds to predict regional stress at low overall loads when the nonuniform load distribution was high (Fig. 3a). This may indicate that near-unloaded or buckled regions of a nonuniformly-loaded tissue can introduce artifacts of higher shear wave propagation speeds on the more highly loaded regions of the tissue. However, the RMSE of predicted regional stress was small (RMSE = 0.55 MPa on average). The extent of the nonuniform loading or stress gradient that can be applied while still accurately resolving regional stress using regional shear wave speed requires further study.

Our second objective was to determine the sensitivity of regional axial stress and regional shear wave speed measurements to nonuniform load distribution and fiber alignment in the presence of variable tissue geometry and constitutive properties. First, we found that unaligned fibers distributed axial stress more uniformly across the tissue during a nonuniform load (Fig. 5). We also found that the interaction between thickness and nonuniform load accounted for much of the variability in regional stress distribution (R^2 = 0.82). However, this is likely due to thinner tissues having a decreased cross-sectional area, and thus a higher axial stress. At higher average axial stresses, regional stresses are more sensitive to nonuniform loading because the fibers are more likely to be in the linear region of the fiber stress-strain response. More notably, we found that errors in predicting regional axial stress based upon regional shear wave speeds were generally independent of all geometric, boundary, and hyperelastic parameters included in this study. We did observe that more highly aligned fibers resulted in greater stress distributions (Fig. 5) and thus greater average stress prediction errors (Fig. 3b), which strongly suggests that shear wave speed is highly sensitive to measurement region in tendon-like tissues undergoing nonuniform loading. This should be a consideration in nonuniform load-bearing tendons, like the Achilles tendon (Franz et al. 2015). In tissues that more effectively distribute stress, like ligament or joint capsule, regional shear wave speed variation may be less of a concern, but experimental follow-ups are needed to confirm.

There are four limitations to consider when interpreting the results presented in this study. First, we implemented a finite element model using a range of parameters commonly found in soft biological tissues, but we did not consider other mechanical phenomena in these tissues that could cause nonuniform loading, such as different hierarchical levels of load transmission like interfibrillar shearing and sliding (Szczesny and Elliott 2014; Rigozzi et al. 2013) or sliding between higher-level tissue constituents such as sub-tendons (Pękala et al. 2017; Ekiert, Tomaszewski, and Mlyniec 2021). However, we expect the results presented in this study to be representative of common structure-scale evaluations of ligaments and tendons. Second, there are numerous anatomical features of biological soft tissues that can give rise to nonuniform axial stress distributions. Here, we only considered linear stress distributions as caused by nonuniform loading, but in biological specimens a non-linear axial stress gradient can be the cause of boundary conditions like the myotendinous junction (Sharafi et al. 2011), bone insertions (Butler et al. 1984; Thomopoulos et al. 2003), or geometric conditions such as changes in cross-section along the tissue length, such as in the Achilles tendon (Magnusson and Kjaer 2003). These conditions during physiological loading can also give rise to buckling in unloaded regions of the tissue, such as in the medial collateral ligament during simple knee flexion (John C. Gardiner, Weiss, and Rosenberg 2001). However, buckled regions of the tissue likely do not carry positive axial stress and are not useful for tensiometry stress measurements. Thus, we did not consider buckling caused by more extreme nonuniform load distributions (i.e., deep knee flexion) in this study. Third, we measured shear wave speeds using a transient analysis and did not consider frequency-dependent phase speeds as measured using shear wave dispersion (Helfenstein-Didier et al. 2016; Brum et al. 2014), which may alter regional shear wave speeds observed in this model and *in vivo.* However, our finding that a simple transient analysis allowed for accurate predictions of regional stress suggests that this analysis can be applied despite the possible dispersive behavior in biological tissues. Finally, shear wave speeds are measured through layers of subcutaneous tissue *in vivo*, which changes the effective density (p_{eff}) of the tissue of interest, and may alter the interpretation of regional shear wave speed at the superficial measurement point (J. L. Blank and Thelen 2023; Sadeghi and Cortes 2020). Whether regional loading can be ascertained using regional wave speeds *in vivo* is an area of ongoing study.

In summary, based on our computational results, regional shear wave speeds are a strong predictor of regional stress in nonuniformly loaded fibrous soft tissues. We found that the regional shear wave speed-stress relationship was independent of factors that change between tissue types, and that this relationship was generally only sensitive to a combination of the degree of nonuniform loading and total tissue load. As such, regional shear wave propagation is a promising measure to gauge regional tissue load directly and objectively.

ACKNOWLEDGMENT

We would like to thank the University of Wisconsin Center for High Throughput Computing for access to their computing resources.

FUNDING

This material is based upon work supported by the National Science Foundation Graduate Research Fellowship Program under Grant No. DGE-1747503. Any opinions, findings, and conclusions or recommendations expressed in this material are those of the author(s) and do not necessarily reflect the views of the National Science Foundation.

NOMENCLATURE

w	Tissue width [mm]
t	Tissue thickness [mm]
ΔF	Nonuniform load distribution [N]
F	Axial load [N]
C_3	Toe region exponential stress coefficient [Mpa]
C_4	Toe region uncrimping term
C_5	Linear region fiber modulus [Mpa]
k_f	Fiber alignment factor
c	Shear wave speed [m/s]
p_{eff}	Effective tissue density [kg/m^3]
μ	Tissue shear modulus [Mpa]
$\sigma_{regional}$	Regional axial stress [Mpa]
$\sigma_{average}$	Average axial stress (*F/A*) [Mpa]
ε_{pred}	Regional stress prediction error [Mpa]
A	Tissue cross-sectional area [mm^2]

REFERENCES

Amis, Andrew A. 1998. “Biomechanics of Bone, Tendon, and Ligament.” In *Sciences Basic to Orthopaedics*, 222–39.

Blank, Jonathon, Matthew Blomquist, Lesley Arant, Stephanie Cone, and Joshua Roth. 2022. “Characterizing Musculoskeletal Tissue Mechanics Based on Shear Wave Propagation - a Systematic Review of Current Methods and Reported Measurements.” *Annals of Biomedical Engineering*. https://doi.org/10.1007/s10439-022-02935-y.

Blank, Jonathon L., and Darryl G. Thelen. 2023. “Adjacent Tissues Reduce Shear Wave Speeds in Axially Loaded Tendons.” *EngrXiv*. https://doi.org/10.31224/2878.

Blank, Jonathon L., Darryl G. Thelen, Matthew S. Allen, and Joshua D. Roth. 2021. “Sensitivity of the Shear Wave Speed-Stress Relationship to Soft Tissue Material Properties and Fiber Alignment.” *Journal of the Mechanical Behavior of Biomedical Materials* 125 (November 2021): 104964. https://doi.org/10.1016/j.jmbbm.2021.104964.

Blank, Jonathon L., Darryl G. Thelen, and Joshua D. Roth. 2020a. “Shear Wave Speeds Track Axial Stress in Porcine Collateral Ligaments.” *Journal of the Mechanical Behavior of Biomedical Materials* 105 (January): 103704. https://doi.org/10.1016/j.jmbbm.2020.103704.

Blank, Jonathon L, Darryl G Thelen, and Joshua D Roth. 2020b. “Ligament Shear Wave Speeds Are Sensitive to Tensiometer-Tissue Interactions: A Parametric Modeling Study.” In *Computer Methods, Imaging and Visualization in Biomechanics and Biomedical Engineering: Selected Papers from the 16th International Symposium CMBBE and 4th Conference on Imaging and Visualization, August 14-16, 2019, New York City, USA*, 36:48–59. https://doi.org/10.1007/978-3-030-43195-2_5.

Brum, J, M Bernal, J L Gennisson, and M Tanter. 2014. “In Vivo Evaluation of the Elastic Anisotropy of the Human Achilles Tendon Using Shear Wave Dispersion Analysis.” *Physics in Medicine and Biology* 59 (3): 505–23. https://doi.org/10.1088/0031-9155/59/3/505.

Butler, DL, ES Grood, FR Noyes, and AN Sodd. 1984. “On the Interpretation of Our Anterior Cruciate Ligament Data.” *Clinical Orthopaedics and Related Research* 196: 26–34.

Cespedes, I., Y. Huang, J. Ophir, and S. Spratt. 1995. “Methods for Estimation of Subsample Time Delays of Digitized Echo Signals.” *Ultrasonic Imaging* 17 (2): 142–71. https://doi.org/10.1006/uimg.1995.1007.

Ekiert, Martyna, Krzysztof A. Tomaszewski, and Andrzej Mlyniec. 2021. “The Differences in Viscoelastic Properties of Subtendons Result from the Anatomical Tripartite Structure of Human Achilles Tendon - Ex Vivo Experimental Study and Modeling.” *Acta Biomaterialia* 125: 138–53. https://doi.org/10.1016/j.actbio.2021.02.041.

Franz, Jason R., Laura C. Slane, Kristen Rasske, and Darryl G. Thelen. 2015. “Non-Uniform in Vivo Deformations of the Human Achilles Tendon during Walking.” *Gait and Posture* 41 (1): 192–97. https://doi.org/10.1016/j.gaitpost.2014.10.001.

Gardiner, J C, and J A Weiss. 2003. “Subject-Specific Finite Element Models Can Predict Strain in the Human Medial Collateral Ligament.” *Journal of Orthopaedic Research* 21: 1098–1106. https://doi.org/10.1016/S0736-0266(03)00113-X.

Gardiner, John C., Jeffrey A. Weiss, and Thomas D. Rosenberg. 2001. “Strain in the Human Medial Collateral Ligament During Valgus Loading of the Knee.” *Clinical Orthopaedics and Related Research* 391 (October): 266–74. https://doi.org/10.1097/00003086-200110000-00031.

Helfenstein-Didier, C., R. J. Andrade, J. Brum, F. Hug, M. Tanter, A. Nordez, and J. L. Gennisson. 2016.

"In Vivo Quantification of the Shear Modulus of the Human Achilles Tendon during Passive Loading Using Shear Wave Dispersion Analysis." *Physics in Medicine and Biology* 61 (6): 2485–96. https://doi.org/10.1088/0031-9155/61/6/2485.

Maas, Steve A, Benjamin J Ellis, Gerard A Ateshian, and Jeffrey A Weiss. 2012. "FEBio: Finite Elements for Biomechanics." *Journal of Biomechanical Engineering* 134 (1): 011005: 1-10. https://doi.org/10.1115/1.4005694.

Magnusson, S. Peter, and Michael Kjaer. 2003. "Region-Specific Differences in Achilles Tendon Cross-Sectional Area in Runners and Non-Runners." *European Journal of Applied Physiology* 90 (5–6): 549–53. https://doi.org/10.1007/s00421-003-0865-8.

Mallett, Kaitlyn F., and Ellen M. Arruda. 2017. "Digital Image Correlation-Aided Mechanical Characterization of the Anteromedial and Posterolateral Bundles of the Anterior Cruciate Ligament." *Acta Biomaterialia* 56: 44–57. https://doi.org/10.1016/j.actbio.2017.03.045.

Martin, Jack A., Scott C.E. Brandon, Emily M. Keuler, James R. Hermus, Alexander C. Ehlers, Daniel J. Segalman, Matthew S. Allen, and Darryl G. Thelen. 2018. "Gauging Force by Tapping Tendons." *Nature Communications* 9 (1): 2–10. https://doi.org/10.1038/s41467-018-03797-6.

Martin, Jack A, Dylan G Schmitz, Alexander C Ehlers, Matthew S Allen, and Darryl G Thelen. 2019. "Calibration of the Shear Wave Speed-Stress Relationship in Ex Vivo Tendons." *Journal of Biomechanics* 90: 9–15. https://doi.org/10.1016/j.jbiomech.2019.04.015.Calibration.

Pękala, P. A., B. M. Henry, A. Ochała, P. Kopacz, G. Tatoń, A. Młyniec, J. A. Walocha, and K. A. Tomaszewski. 2017. "The Twisted Structure of the Achilles Tendon Unraveled: A Detailed Quantitative and Qualitative Anatomical Investigation." *Scandinavian Journal of Medicine and Science in Sports* 27 (12): 1705–15. https://doi.org/10.1111/sms.12835.

Readioff, Rosti, Brendan Geraghty, Eithne Comerford, and Ahmed Elsheikh. 2020. "A Full-Field 3D Digital Image Correlation and Modelling Technique to Characterise Anterior Cruciate Ligament Mechanics Ex Vivo." *Acta Biomaterialia* 113: 417–28. https://doi.org/10.1016/j.actbio.2020.07.003.

Rigozzi, S., R. Müller, A. Stemmer, and J. G. Snedeker. 2013. "Tendon Glycosaminoglycan Proteoglycan Sidechains Promote Collagen Fibril Sliding-AFM Observations at the Nanoscale." *Journal of Biomechanics* 46 (4): 813–18. https://doi.org/10.1016/j.jbiomech.2012.11.017.

Robinson, J. R., J. Sanchez-Ballester, A. M. J. Bull, R. de W. M. Thomas, and A. A. Amis. 2004. "The Posteromedial Corner Revisited." *The Journal of Bone and Joint Surgery. British Volume* 86-B (5): 674–81. https://doi.org/10.1302/0301-620x.86b5.14853.

Sadeghi, Seyedali, and Daniel H. Cortes. 2020. "Measurement of the Shear Modulus in Thin-Layered Tissues Using Numerical Simulations and Shear Wave Elastography." *Journal of the Mechanical Behavior of Biomedical Materials* 102 (October 2019). https://doi.org/10.1016/j.jmbbm.2019.103502.

Sharafi, Bahar, Elizabeth G. Ames, Jeffrey W. Holmes, and Silvia S. Blemker. 2011. "Strains at the Myotendinous Junction Predicted by a Micromechanical Model." *Journal of Biomechanics* 44 (16): 2795–2801. https://doi.org/10.1016/j.jbiomech.2011.08.025.

Stender, Christina J., Evan Rust, Peter T. Martin, Erica E. Neumann, Raquel J. Brown, and Trevor J. Lujan. 2018. "Modeling the Effect of Collagen Fibril Alignment on Ligament Mechanical Behavior." *Biomechanics and Modeling in Mechanobiology* 17 (2): 543–57. https://doi.org/10.1007/s10237-017-0977-4.

Szczesny, Spencer E., and Dawn M. Elliott. 2014. "Interfibrillar Shear Stress Is the Loading Mechanism of Collagen Fibrils in Tendon." *Acta Biomaterialia* 10 (6): 2582–90. https://doi.org/10.1016/j.actbio.2014.01.032.

Thomopoulos, Stavros, Gerald R. Williams, Jonathan A. Gimbel, Michele Favata, and Louis J. Soslowsky. 2003. "Variation of Biomechanical, Structural, and Compositional Properties along the Tendon to Bone Insertion Site." *Journal of Orthopaedic Research* 21 (3): 413–19. https://doi.org/10.1016/S0736-0266(03)0057-3.

Willinger, Lukas, Shun Shinohara, Kiron K. Athwal, Simon Ball, Andy Williams, and Andrew A. Amis. 2020. "Length-Change Patterns of the Medial Collateral Ligament and Posterior Oblique Ligament in Relation to Their Function and Surgery." *Knee Surgery, Sports Traumatology, Arthroscopy* 28 (12): 3720–32. https://doi.org/10.1007/s00167-020-06050-0.

Wymenga, A. B., J. J. Kats, J. Kooloos, and B. Hillen. 2006. "Surgical Anatomy of the Medial Collateral Ligament and the Posteromedial Capsule of the Knee." *Knee Surgery, Sports Traumatology, Arthroscopy* 14 (3): 229–34. https://doi.org/10.1007/s00167-005-0682-1.

Regional Shear Wave Speeds Track Regional Axial Stress in Nonuniformly Loaded Fibrous Soft Tissues – *Supplementary Materials*

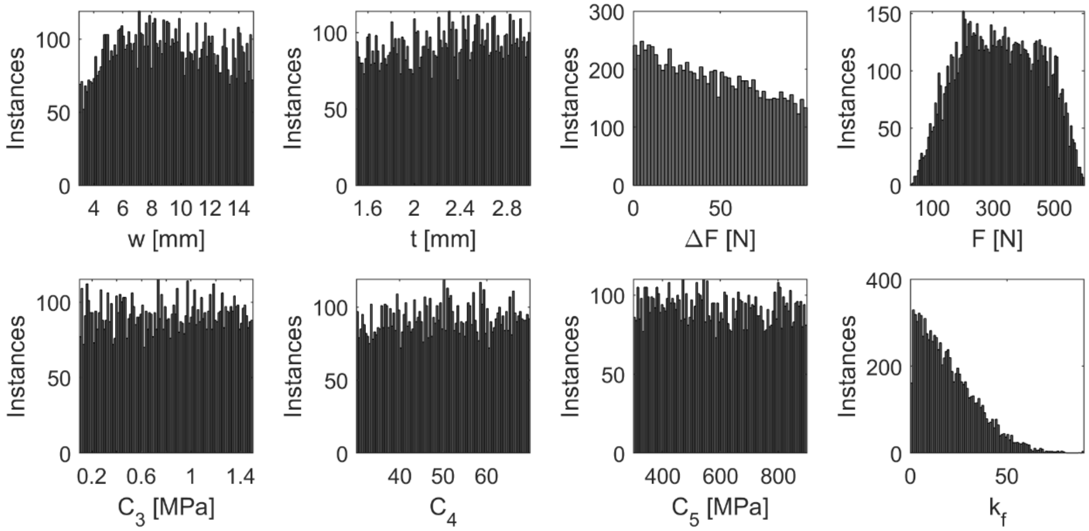

Figure 1S: Histogram plots represent the number of simulations with the corresponding input parameters. All parameters but k_f were specified using a random uniform distribution. The value of ΔF was constrained such that it did not exceed 100 N, and F (total force applied) was constrained such that it was between 0 and 600 N.

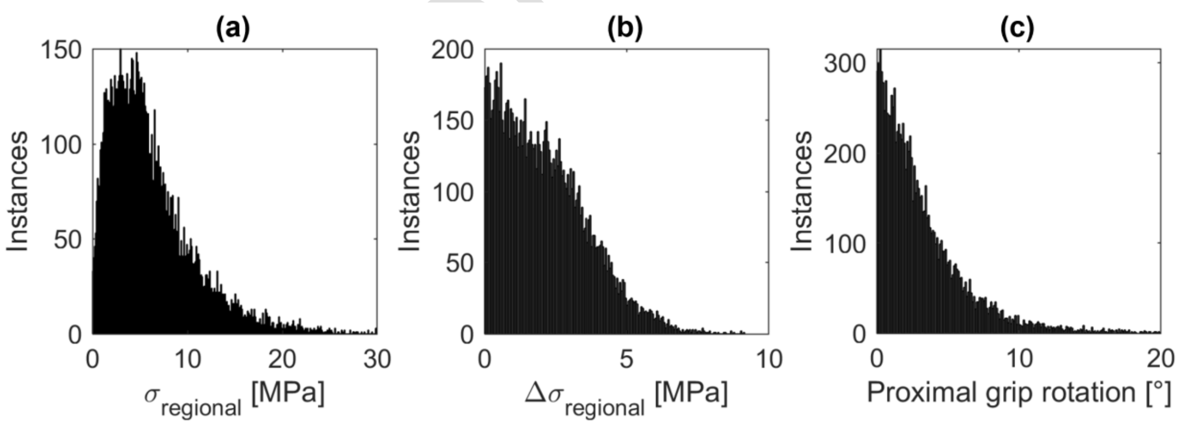

Figure 2S: Histogram plots represent the number of simulations with the corresponding output parameters. **(a)** We observed regional stresses that generally ranged from 0 to 20 MPa. **(b)** The regional stress gradient across the tissue width generally ranged up to 5 MPa. **(c)** The proximal grip of the tissue generally rotated between 0 and 10° due to the nonuniform load gradient.

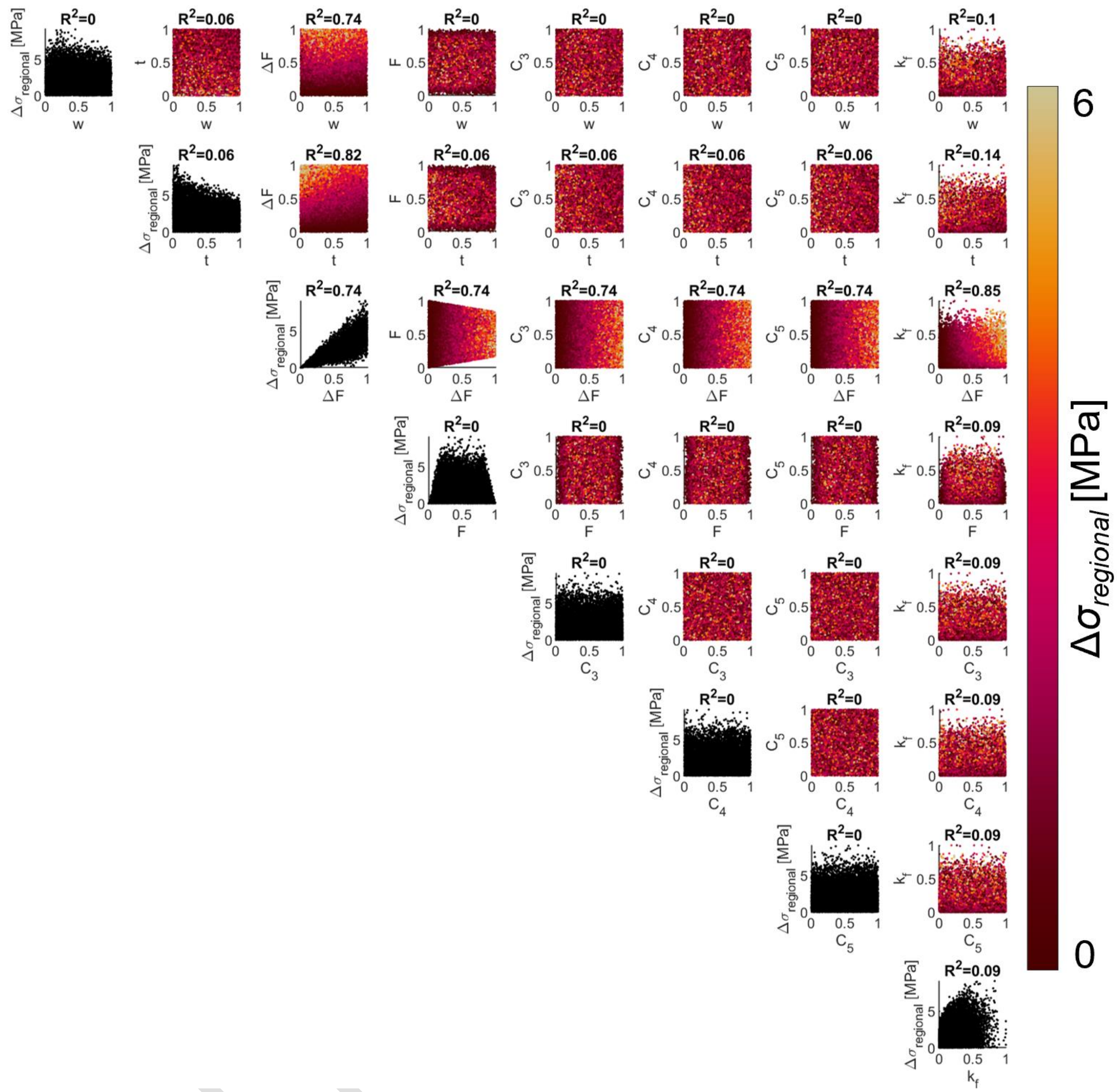

Figure 3S: Sensitivity of regional stress distribution, $\Delta\sigma_{regional}$ to normalized parameter ranges. Shown in diagonal plots are the percentage of variability of $\Delta\sigma_{regional}$ accounted for by a single parameter (R^2), and the slope of a linear regression fit (in MPa/parameter range). Also shown are one-way interactions (off-diagonal) between each set of primary factors with the colormap indicating $\Delta\sigma_{regional}$.

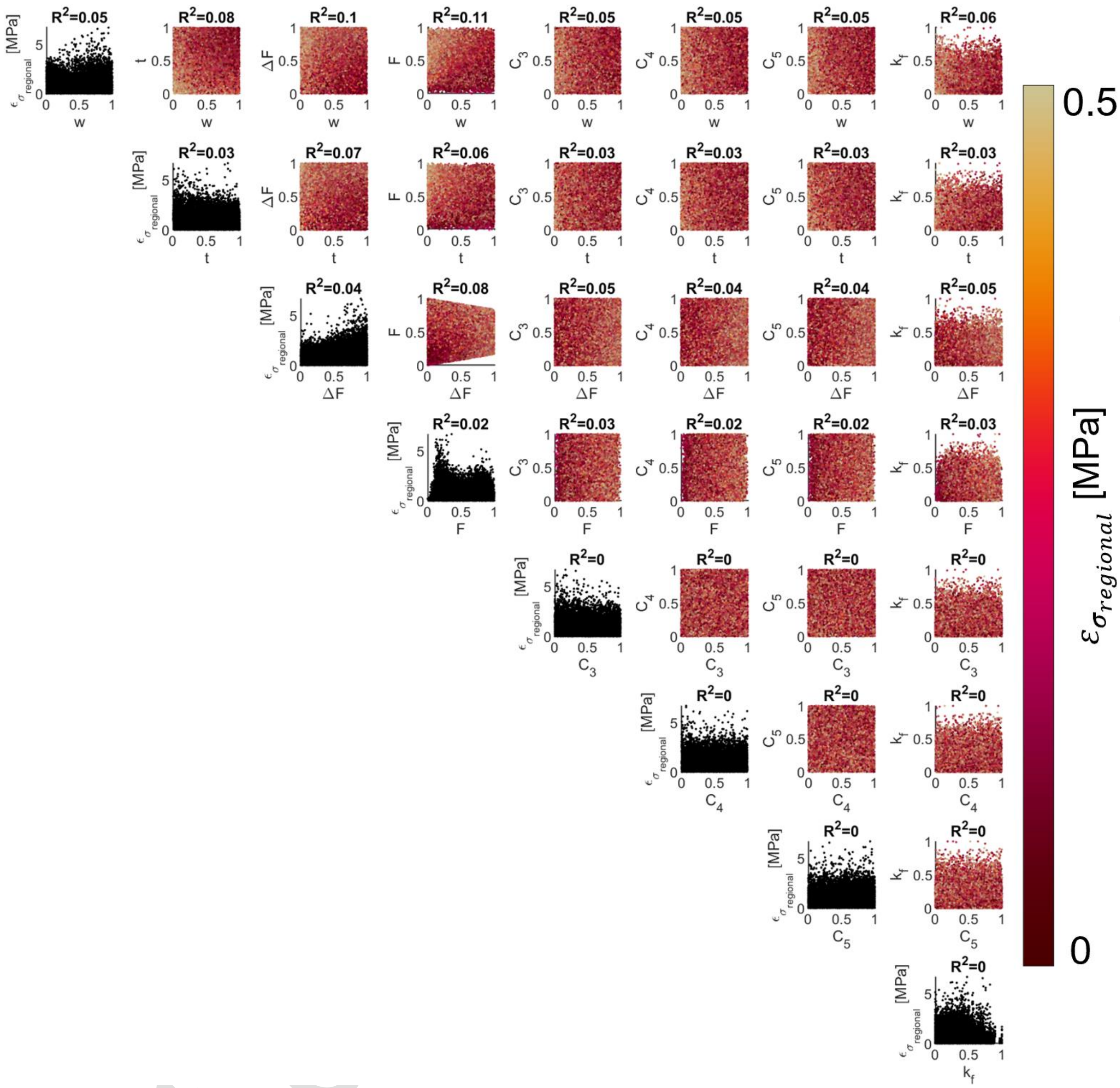

Figure 4S: Sensitivity of regional stress distribution, $\varepsilon_{\sigma_{regional}}$ to normalized parameter ranges. Shown in diagonal plots are the percentage of variability of $\varepsilon_{\sigma_{regional}}$ accounted for by a single parameter (R^2), and the slope of a linear regression fit (in MPa/parameter range). Also shown are one-way interactions (off-diagonal) between each set of primary factors with the colormap indicating $\varepsilon_{\sigma_{regional}}$.

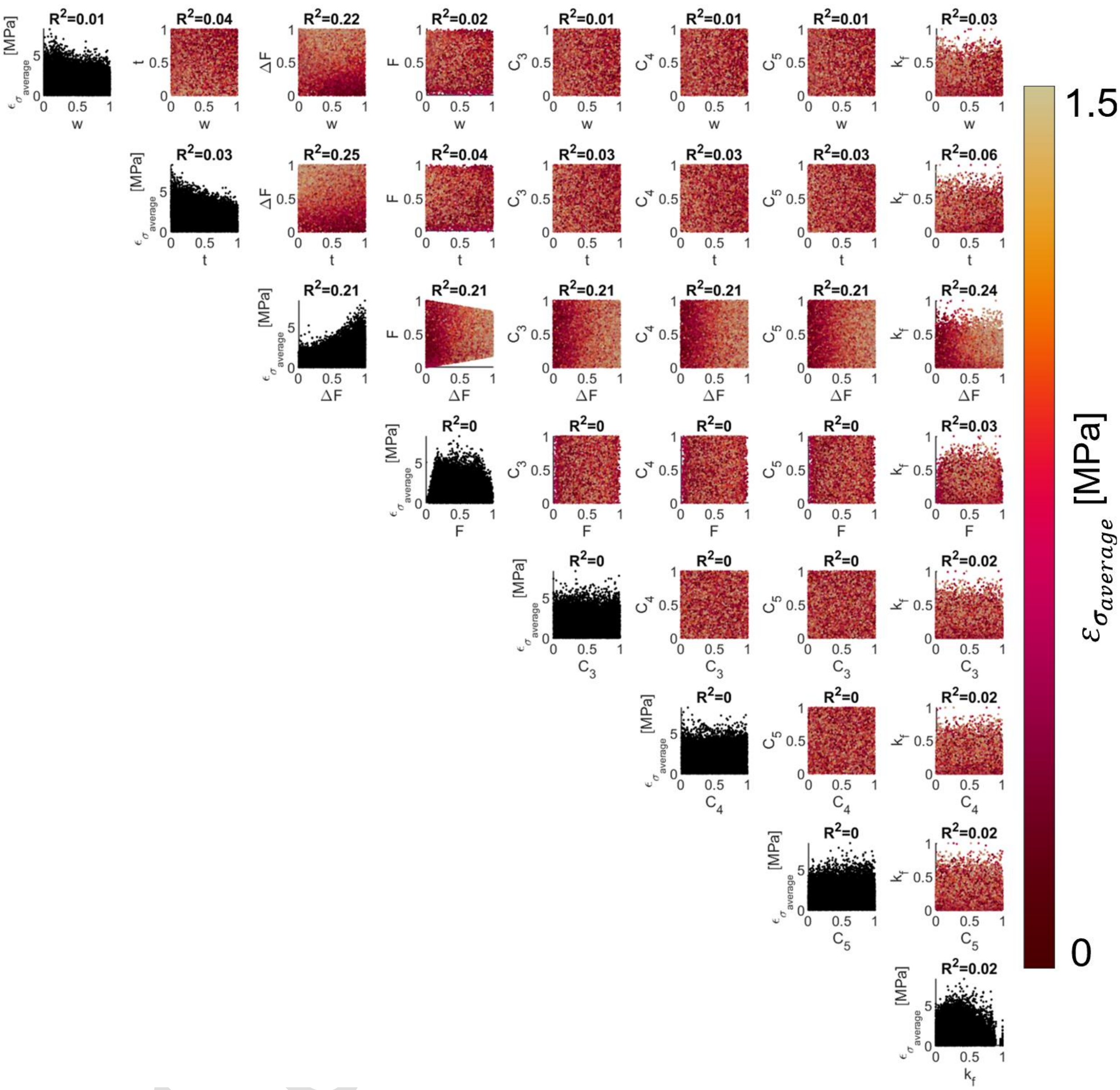

Figure 5S: Sensitivity of regional stress distribution, $\varepsilon_{\sigma_{average}}$ to normalized parameter ranges. Shown in diagonal plots are the percentage of variability of $\varepsilon_{\sigma_{average}}$ accounted for by a single parameter (R^2), and the slope of a linear regression fit (in MPa/parameter range). Also shown are one-way interactions (off-diagonal) between each set of primary factors with the colormap indicating $\varepsilon_{\sigma_{average}}$.

Table 1S: Sensitivity of varied parameters (normalized) on regional stress distribution (reported in MPa/unit increase in parameter) for $\varepsilon_{\sigma_{regional}}$ and $\varepsilon_{\sigma_{average}}$. Sensitivities are reported in MPa/unit increase in parameter.

	w	***t***	***ΔF***	***F_l***	***C_3***	***C_4***	***C_5***	***k_f***
$\varepsilon_{\sigma_{regional}}$ [MPa/range]	-0.33	-0.25	0.31	0.27	-0.03	-0.02	-0.002	0.13
$\varepsilon_{\sigma_{average}}$ [MPa/range]	-0.29	-0.49	1.24	0.20	-0.04	-0.003	0.07	0.71